Superconductor Science and Technology

PAPER

Proposal of an effective mechanical reinforcement structure for a REBaCuO disk bulk pair by full metal encapsulation to achieve a higher trapped field over 20 T

Supercond. Sci. Technol. **32** (2019) 045005 (9pp) https://doi.org/10.1088/1361-6668/ab0017

Proposal of an effective mechanical reinforcement structure for a REBaCuO disk bulk pair by full metal encapsulation to achieve a higher trapped field over 20 T

Hiroyuki Fujishiro[1], **Tomoyuki Naito**[1] and **Satoshi Awaji**[2]

[1] Faculty of Science and Engineering, Iwate University, Morioka 020-8551, Japan
[2] High Field Laboratory for Superconducting Materials (HFLSM), Institute for Materials Research, Tohoku University, Sendai 980-8577, Japan

E-mail: fujishiro@iwate-u.ac.jp

Received 19 October 2018, revised 16 January 2019
Accepted for publication 18 January 2019
Published 25 February 2019

Abstract

In this paper, we propose an effective mechanical reinforcement of a REBaCuO superconducting disk bulk pair to avoid mechanical fracture due to a large hoop stress during field-cooled magnetization (FCM), and confirm the reinforcement effect using numerical simulation. In this reinforcement, the disk bulk is fully encapsulated by an outer metal ring with upper and lower plates made by stainless steel (SUS316). The trapped field, B_z, in the bulk pair with various critical current densities, J_c, was numerically simulated during FCM from $B_{app} = 22$ T, and the hoop stress, σ_θ, was also estimated during FCM after cooling from 300 to 20 K. As a result, the trapped field of over 20 T can be achieved in the gap center of the bulk pair. A large compressive hoop stress, σ_θ^{cool}, due to the difference of thermal expansion coefficients between the bulk and stainless steel, was effectively applied to the whole bulk during the cooling process, compared to that for the conventional reinforcement using only a SUS316 outer ring. The electromagnetic hoop stress, $\sigma_\theta{}^{FCM}$, during FCM was also reduced, and the maximum of the total hoop stress, σ_θ^{total} ($= \sigma_\theta{}^{FCM} + \sigma_\theta^{cool}$), can be reduced below the fracture strength of the REBaCuO bulk. The possibility to achieve a higher trapped field over 20 T is suggested in the gap of the REBaCuO bulk pair without mechanical fracture.

Keywords: field cooled magnetization, numerical simulation, mechanical reinforcement, higher trapped field, mechanical stress

(Some figures may appear in colour only in the online journal)

1. Introduction

The superconducting characteristics of $REBa_2Cu_3O_y$ bulks (REBaCuO, RE: rare earth element or Y) have been recently enhanced due to the introduction of strong pinning centers and the improvement of the crystal growth technique, which results in increased critical current densities, J_c [1, 2]. As a result, the bulks have a significant potential as high-field trapped field magnets (TFMs). However, it is not an exaggeration to say that the maximum of the reported trapped field at lower temperatures was not determined by the superconducting characteristics, but by mechanical strength of the bulk. Because the REBaCuO bulk is a brittle ceramic material, and has a lower mechanical strength than the larger hoop stress due to the Lorentz force during the magnetization process. Since the REBaCuO bulk superconductor is also a composite material, in which the RE_2BaCuO_5 (RE211), Pt and Ag particles are dispersed in the $REBa_2Cu_3O_7$ (RE123) quasi-single crystal matrix with a layered structure, the stress concentration is likely to take place around the so called secondary phases. In addition, the bulk contains a significant number of imperfections such as grain boundaries, crystalline defects, inclusions, voids, and so on, which may cause the stress concentration in local regions and may initiate small local cracks. Additionally, micro-cracks along the *ab*-plane formed during post-annealing treatment of oxygenation are a common ingredient in the microstructure [3–7]. These weak points should also severely reduce the mechanical strength of the material, as they are the starting points for further cracking under tensile stress. As a result, the mechanical stress is concentrated at the weak points, which has a lower mechanical strength, and the bulk would ultimately break and the actual destruction of the REBaCuO bulk is likely to happen from the mechanically weak points in the bulk material during the magnetizing and cooling process.

For YBaCuO bulks, a relatively low tensile strength of about $\sigma_{max} \sim 25$ MPa has been found, which was limited by the initial size of the small cracks produced by the crystal growth [8]. The ring-shaped bulk, in particular, suffers from higher mechanical stress, compared to the disk bulk, because of the concentration of the hoop stress at the innermost periphery [9]. To avoid mechanical fracture, the increase of internal tensile strength by the addition of Ag in the YBaCuO bulk was reported up to 30–40 MPa [10], up to 70 MPa [11] and even up to 115 MPa for the GdBaCuO bulk [12], all of which were measured by bending tests. The epoxy resin impregnation is also an effective way to enhance the mechanical strength, in which voids near the bulk surface are filled with the epoxy resin [13–15]. Another way to improve the internal mechanical properties is the elimination of voids, which were reduced by increasing the O_2 pressure in the post-annealing after the crystal growth [16]. Both the fracture strength and Young's modulus of the REBaCuO bulk were increased with decreasing contents of voids [17–19]. For the void-free and crack-free microstructure of YBaCuO bulk superconductors, its mechanical strength was estimated to be higher than 300 MPa, suggesting a possible trapped field of over 30 T without fracture [20].

A complementary approach to avoid cracking during magnetization process is to encapsulate the bulk in steel tube externally [21], which leads to stress compensation by generating a compressive stress on the bulk after cooling from 300 K to the magnetizing temperature due to the thermal expansion coefficient of the steel larger than the one of REBaCuO in the *ab*-plane. Using the steel ring encapsulation, a trapped field of 14.4 T was reported at 22 K in the gap between Ag-doped YBaCuO disks [21] and of 16 T at 24 K [22]. A trapped field value of 17.24 T at 29 K was reported in an arrangement of two YBaCuO bulks of 26 mm in diameter with impregnated with wood's metal and resin and reinforced by carbon fibre [13], in which a dome-like trapped field profile can be seen. The flat part of the profile suggests that the bulk has a larger J_c value to achieve a trapped field higher than 20 T at 29 K under the sufficient reinforcement. The record-high trapped field has been updated to 17.60 T at 26 K in the gap between two GdBaCuO disks 25 mm in diameter, reinforced by shrink-fit steel [23], in which the reinforcement effect of the shrink-fit steel was simply estimated for the disk bulk and steel ring with infinite height. In this way, the mechanical reinforcement of the bulk is the key technique to achieve higher trapped field in the REBaCuO TFMs.

It is important to analyze the mechanical stress numerically in the bulk during magnetization process. The analytical solutions of the trapped field and mechanical stress of the TFM were reported using the expanded theory for the bulk cylinder with infinite height [8]. The similar analytical solutions of the flux-pinning-induced stress and strain distributions in the infinite bulk cylinder and ring bulk were presented during field-cooled magnetization (FCM) and zero-field cooled magnetization [24–26]. The magnetostriction of superconducting cylinders and rings with finite height was also reported during FCM by the finite element method [27]. However, these papers were based on Bean's critical state model for a *c*-axis oriented, infinite superconducting cylinder, in which the critical current density, J_c, is independent of the magnetic field.

Recently, we have investigated the numerical simulation of the trapped field, B_z, and the mechanical stresses (hoop stress, σ_θ, and radial stress, σ_r) in the REBaCuO ring bulk with finite height reinforced by a metal ring with the same height during FCM [28, 29]. The thermal compressive stress, σ_θ^{cool}, which occurs in the ring bulk when cooling down to operating temperature due to the difference of thermal expansion coefficient between the bulk material and metal ring, was effectively applied at the center of the bulk. However, the σ_θ^{cool} value was reduced comparatively at the uppermost surface of the ring bulk because of a larger thermal contraction of the metal ring along the height direction besides the radial direction. These results suggest that the reinforcement effect by metal ring becomes weak at the surface of the bulk with finite height, and the bulk might break due to the large Lorentz force during FCM from the higher magnetic field. We have recently proposed a new reinforcement structure using an aluminum alloy ring to the annular REBaCuO bulks applicable to compact and cryogen-free 400 MHz (9.4 T) nuclear magnetic resonance spectrometer using a numerical simulation, in which the surface metal plate molded to the metal ring at the uppermost ring bulk is effective to reduce the hoop stress [30]. We believe that a higher trapped field over 20 T can be also achieved in the bulk pair reinforced by a suitable reinforcement structure.

In this paper, we propose an effective mechanical reinforcement structure for the REBaCuO disk bulk and perform the numerical simulation for the trapped field and the hoop stress, σ_θ, in the bulk pair, compared to those of the bulk pair reinforced by conventional metal ring with the same height as the disk bulk. The possibility to achieve a higher trapped field over 20 T is suggested in the gap of the REBaCuO disk bulks without fracture.

2. Numerical simulation procedure

Based on our experimental setup for the FCM procedure at the High Field Laboratory for Superconducting Materials, Institute for Materials Research, Tohoku University, we prepared the following framework of three-dimensional numerical simulation for electromagnetic and mechanical properties. A schematic view of the numerical model using a new reinforcement structure is presented in figure 1(a). Two REBaCuO disk bulks

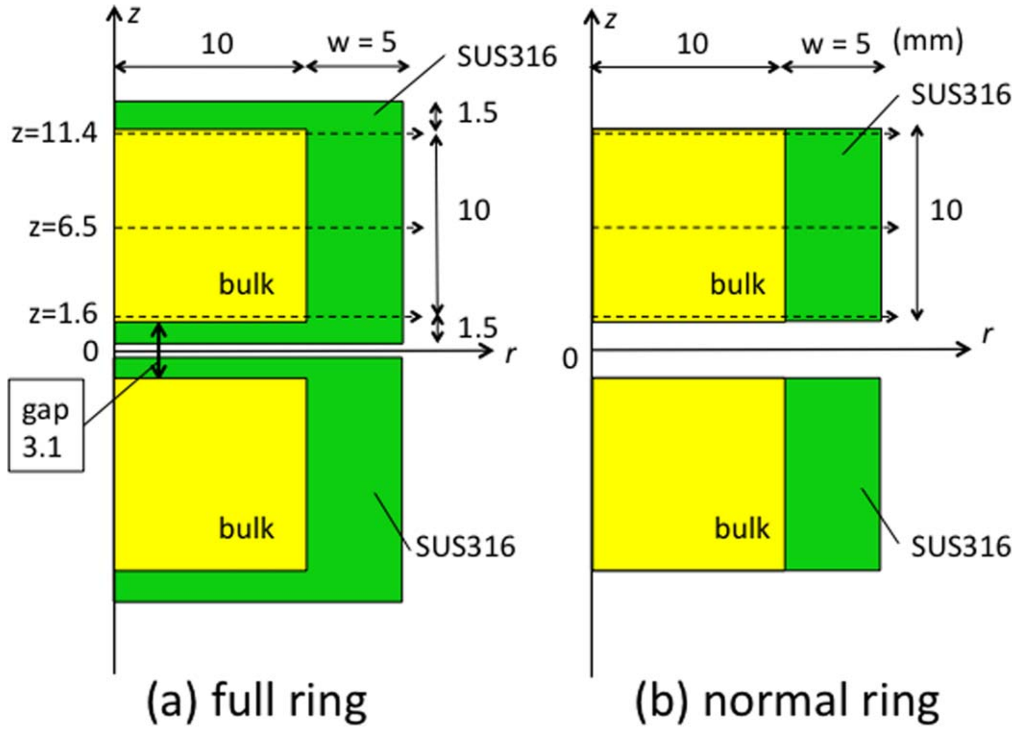

Figure 1. Schematic view of the numerical model of (a) the proposed reinforcement structure named 'full ring' and (b) the conventional reinforcement structure named 'normal ring'.

(20 mm in diameter and 10 mm in height) were fully surrounded by a stainless steel (SUS316) ring 5 mm in width ($w = 5$ mm) and upper and lower SUS316 plates 1.5 mm thick. We abbreviate the fully encapsulated disk bulks as 'full ring'. Then, two bulk modules were stacked with a gap of 0.1 mm along the z-direction and were magnetized by FCM at $T_s = 20$ K using an infinite solenoid coil (150 mm outer diameter, 100 mm inner diameter and infinite height), in which the distance between two bulks is 3.1 mm. For comparison of the reinforcement effect, a schematic model for a conventional reinforcement is presented in figure 1(b), in which two bulk disks are bundled by SUS316 ring 5 mm in width and stacked with a gap of 3.1 mm. We abbreviate this disk bulks as 'normal ring'. In these numerical models, the interface between the bulk and SUS316 part was fixed perfectly. Physical phenomena in the simulation during FCM are described using an electromagnetic equation [28–30], in which temperature is assumed to be constant for simplicity. The simulation results of the trapped field, B_z, depend strongly on the temperature and magnetic field dependence of critical current density, $J_c(T, B)$, of the superconducting bulk [31]. To achieve the trapped field of $B_z^* = 22$ T in the infinite height bulk 20 mm in diameter, $J_c^* = 1.752 \times 10^9$ A m^{-2} is necessary under the relation of $B_z^* = \mu_0 J_c^* R$ (R: radius of the disk bulk) by Bean's critical state model. However, for the actual finite height bulk, the J_c of the bulk must be higher than J_c^* to achieve $B_z = 22$ T at $B_{app} = 22$ T, because the induced superconducting current flows fully in the upper and lower bulk surface.

Kii *et al* measured the temperature and magnetic field dependence of critical current density, $J_c(T, B)$, of the GdBaCuO bulk at low temperatures, which was determined

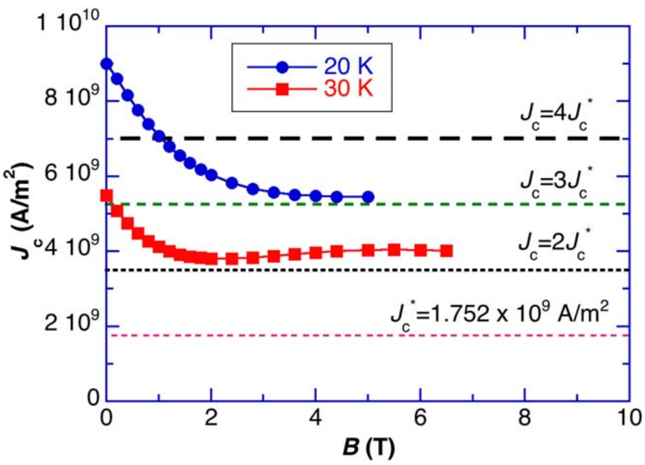

Figure 2. The reported $J_c(T, B)$ profiles of GdBaCuO bulk at 20 K and 30 K by Kii *et al* [32]. The J_c values used in the present simulation; $J_c = 2J_c^* = 3.503 \times 10^9$ A m^{-2}, $J_c = 3J_c^* = 5.254 \times 10^9$ A m^{-2}, and $J_c = 4J_c^* = 7.006 \times 10^9$ A m^{-2}, which are assumed to be constant under magnetic field.

using the extended Bean's model for magnetic moment hysteresis (M–H) loops measured by a SQUID magnetometer under the applied field parallel to the c-axis of a small sample without cracks [32]. Figure 2 shows the fitted $J_c(T, B)$ curves at 20 and 30 K by Kii *et al.* The J_c increases with decreasing temperature and decreases with increasing magnetic field, which shows weaker magnetic field dependence, compared to the one at higher temperature [32]. The trapped field, B_z, on the single finite bulk surface estimated using the measured

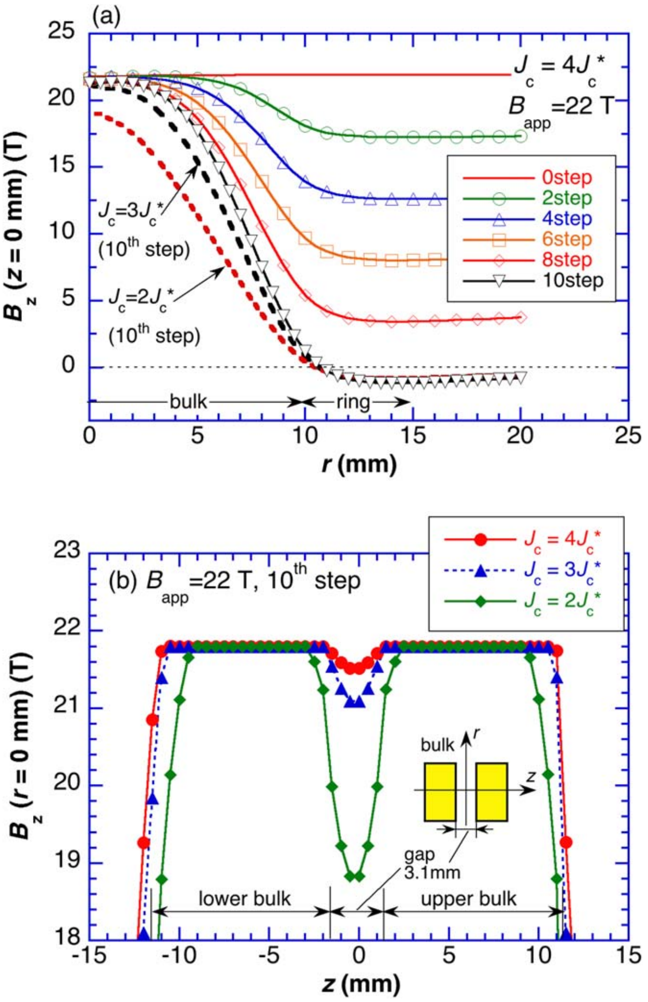

Figure 3. (a) Time step dependence of the cross section of the trapped field profile during FCM from $B_{app} = 22$ T in the gap center of two bulks along the r-direction, $B_z(z = 0$ mm), for the case of $J_c = 4J_c^*$. The final $B_z(z = 0$ mm) profiles of 10th step for the cases of $J_c = 3J_c^*$ and $2J_c^*$ were also shown. (b) $B_z(r = 0$ mm) profiles of the 10th step for each J_c case along the z-direction.

$J_c(T, B)$ value is generally overestimated, and the J_c also decreases along the bulk radius because the quality decreases with the growth front progression [33]. From this evidence, the magnitude of $J_c(B)$ should be adjusted to one third of its small specimen value to adequately reproduce the trapped field by FCM [34, 35]. In the present simulation, the trapped field, B_z, is estimated in the bulk pair to eliminate the demagnetization effect and the J_c value is assumed to be $2J_c^*$, $3J_c^*$ and $4J_c^*$, as shown in figure 2, which is independent of applied magnetic field.

The power-n model was used to describe the nonlinear E–J characteristic of the superconducting bulk:

$$E = E_c\left(\frac{J}{J_c}\right)^n, \tag{1}$$

where E_c ($= 10^{-4}$ V m^{-1}) is the reference electric field and J_c is the critical current density. To realize the approximate Bean's model, a large n value ($n = 100$) and a constant J_c are assumed in equation (1) [28]. In the simulation process of FCM, a magnetic field of $B_{app} = 22$ T was applied above the critical temperature, T_c ($= 92$ K), and then the bulk was cooled to $T_s = 20$ K. Thereafter, the magnitude of the magnetic field was monotonically decreased from 22 T to zero by ten steps with -0.15 T min^{-1}, which is a ramp rate used in our experiments. The time step (TS) of the descent of magnetic field during FCM is defined as follows

Table 1. Mechanical parameters used in the numerical simulation (E: Young's modulus, ν: Poisson ratio, α: thermal expansion coefficient) [9, 28].

	E (GPa)	ν	α (K^{-1})
REBaCuO bulk	100	0.33	5.2×10^{-6}
SUS316	193	0.28	1.27×10^{-5}

$$\mathrm{TS} = 10\frac{B_{app} - B_{ex}}{B_{app}}, \tag{2}$$

where B_{ex} is the actual external magnetic field.

In an isotropic material, Hooke's law is established, in which the stress is linearly proportional to the strain. Although the actual REBaCuO bulk is mechanically anisotropic and inhomogeneous, as already mentioned in section 1, the mechanical properties of the REBaCuO bulk are assumed to be isotropic and homogeneous for simplicity. The electromagnetic hoop stress, σ_θ^{FCM}, was calculated for each step of FCM, which acts circumferentially on each end face of the meshed element [8, 24]. The thermal hoop stress, σ_θ^{cool}, by cooling from 300 to 20 K was also calculated, which was generated by the difference of the thermal expansion coefficient, α, between the REBaCuO bulk and the SUS316 ring. The mechanical parameters (Young's modulus, E, Poisson ratio, ν, and thermal expansion coefficient, α) of the REBaCuO bulk and SUS316 used in the elastic simulation are summarized in table 1, in which E and ν values are those at 300 K and are assumed to be independent of temperature [9, 29], although the mechanical strength such as bending strength of the REBaCuO bulk slightly increases with decreasing temperature due to the decrease of the inter-atomic distance by cooling [16]. Commercial software package, Photo-EDDY (Photon Ltd, Japan) was used for the analysis of the distributions of magnetic field, B_z, along z-direction and the induced persistent current density, J_θ, the circumferential (θ) direction during FCM. The σ_θ^{FCM} and σ_θ^{cool} values were calculated for each step by Photo-ELAS (Photon Ltd, Japan) using the nodal force at each node calculated by Photo-EDDY. In the model, the bulk enclosed by the SUS316 part was equally divided into 36 elements along the θ-direction and by the 0.5 mm pitch along the r- and z-directions.

3. Numerical simulation results

3.1. Electromagnetic properties

Figure 3(a) shows the TS dependence of the cross section of the trapped field profile, $B_z(r)$, during FCM from $B_{app} = 22$ T in the gap center of two bulks along the r-direction at $z = 0$,

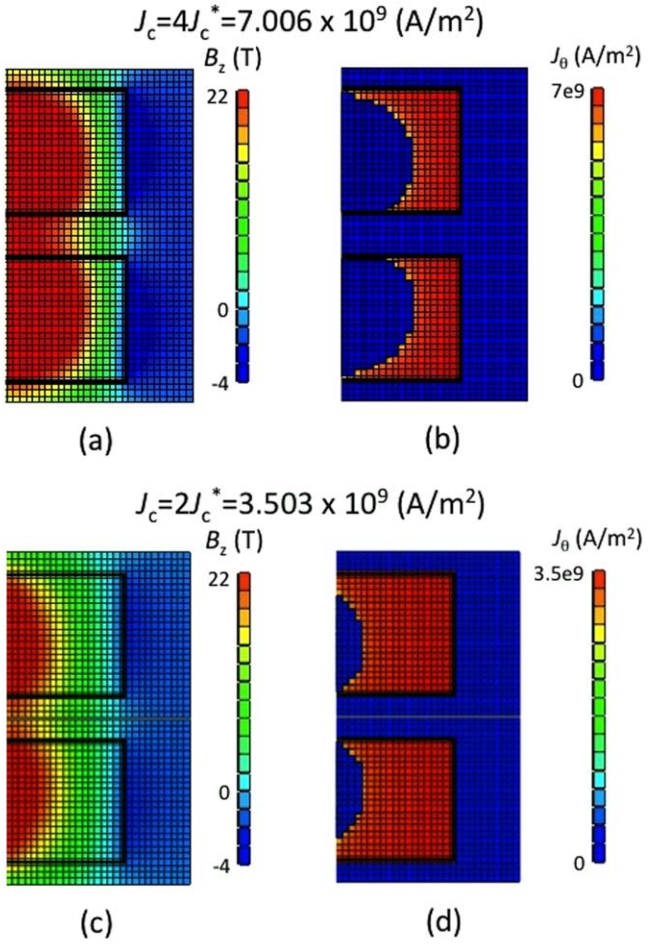

Figure 4. The final (10th step) contour maps of the (a) trapped field, B_z, and (b) persistent current density, J_θ, in the pair of bulk module for $J_c = 4J_c{}^*$ during FCM from $B_{app} = 22$ T. The similar contour maps of (c) B_z and (d) J_θ profiles for $J_c = 2J_c{}^*$ during FCM from $B_{app} = 22$ T.

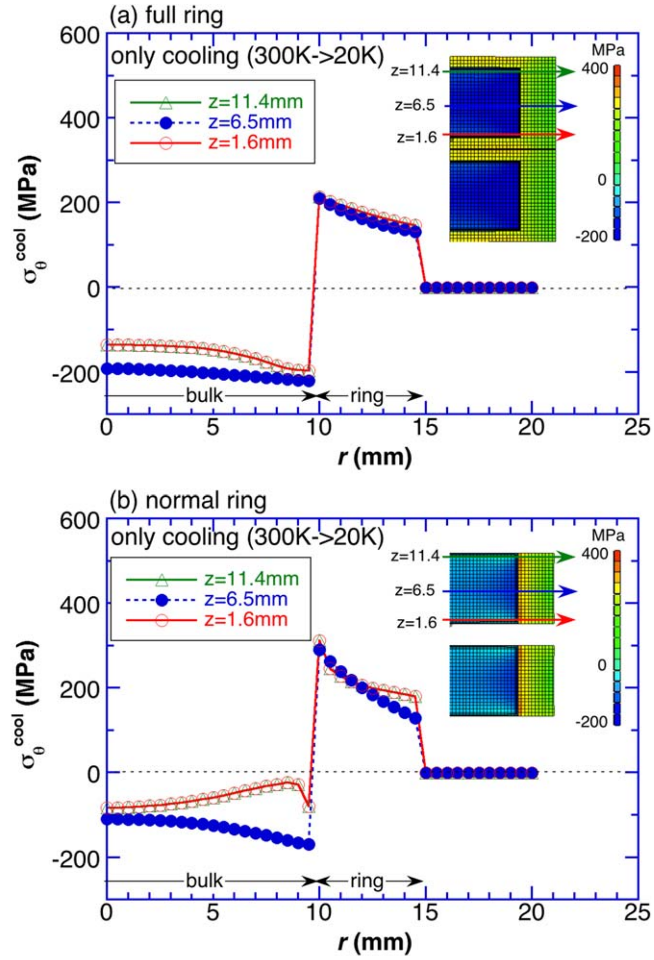

Figure 5. The radius (r) dependence of the thermal hoop stress, $\sigma_\theta{}^{cool}$, for the (a) 'full ring' and (b) 'normal ring' at various z-positions under the cooling from 300 K to 20 K without FCM. The inset of each figure shows the contour map of the $\sigma_\theta{}^{cool}$ profile.

for the case of $J_c = 4J_c{}^* = 7.006 \times 10^9$ A m^{-2}. The external magnetic field decreased step by step without a field slope due to the infinite length of magnetizing solenoid coil. The $B_z(r)$ value in the bulk also decreased step by step, but $B_z(r)$ for $r < 2$ mm kept a constant value of 21.8 T, which was nearly the same value as B_{app}. These results suggest that the bulk was not fully magnetized due to the larger J_c $(= 4J_c{}^*)$ value, that is, the induced supercurrent partially flows in the periphery region. In the figure, the final $B_z(r)$ profiles of the 10th step at $z = 0$ mm for the cases of $J_c = 3J_c{}^*$ and $2J_c{}^*$ are also shown, in which the constant $B_z(r)$ region became narrow and $B_z(z = 0$ mm) decreased with decreasing J_c, because the persistent supercurrent flowing region became wide. Figure 3(b) shows the final (10th step) trapped field profile, $B_z(z)$, along the z-direction ($r = 0$ mm) for each J_c value. For $J_c = 4J_c{}^*$, the decrease of B_z at the gap center, ΔB_z, is as small as 0.3 T ($B_z(r = z = 0$ mm) = 21.5 T). However, ΔB_z was 0.74 T ($B_z(r = z = 0) = 21.06$ T) for $J_c = 3J_c{}^*$ and 2.98 T ($B_z(r = z = 0$ mm) = 18.82 T) for $J_c = 2J_c{}^*$. To achieve higher B_z in the central gap, the J_c value should be increased and the width of the gap between the bulks should be minimized.

Figures 4(a) and (b), respectively, show the contour maps of the final (10th step) trapped field, B_z, and the persistent current density, J_θ, in the bulk pair for $J_c = 4J_c{}^*$ during FCM from $B_{app} = 22$ T. In figure 4(b), the persistent supercurrent, which is as large as $4J_c{}^*$, flows along the θ-direction in outer region and top and bottom surfaces of the bulk pair. As a result, the magnetic field was profiled as shown in figure 4(a), which was closely correlated with the J_θ profile. Figures 4(c) and (d), respectively, show the similar contour plots of the 10th step B_z, and J_θ in the bulk pair for $J_c = 2J_c{}^*$ during FCM from $B_{app} = 22$ T. The region, at which the persistent supercurrent with $2J_c{}^*$ flows, became wider, compared to that for the $J_c = 4J_c{}^*$ case. As a result, the region with higher B_z value became narrow and the B_z value at the gap center decreased.

3.2. Mechanical properties

Figures 5(a) and (b), respectively, show the radius (r) dependence of the thermal hoop stress, σ_θ^{cool}, for the 'full ring' and the 'normal ring' cases at various z-positions under the cooling from 300 to 20 K without FCM (only cooling). The

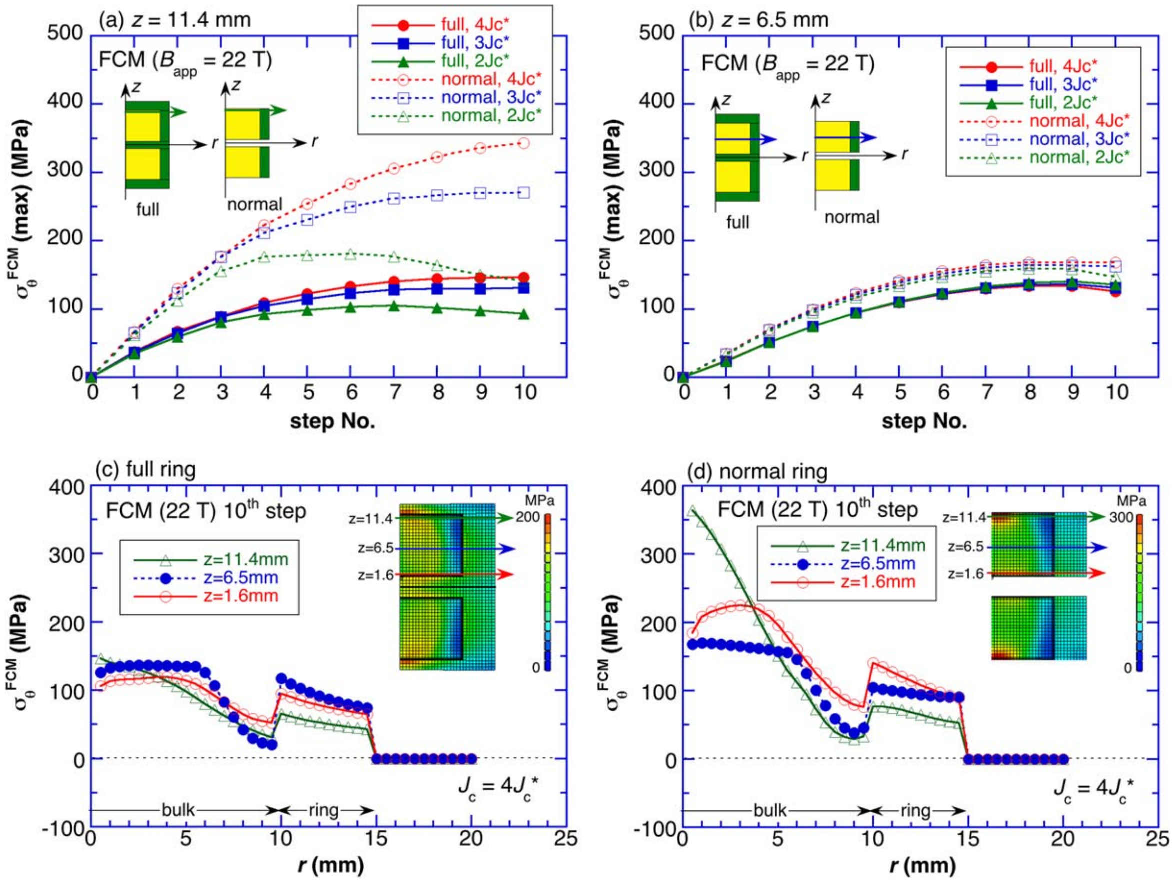

Figure 6. The time step (TS) dependence of the $\sigma_\theta{}^{\rm FCM}$ values at the positions of (a) $(r, z) = (0.5$ mm, 11.4 mm) and (b) $(r, z) = (0.5$ mm, 6.5 mm) for the 'full ring' and the 'normal ring' cases under $J_c = 2J_c{}^*$, $3J_c{}^*$ and $4J_c{}^*$ during FCM from 22 T without cooling (only FCM). The radius (r) dependence of the $\sigma_\theta{}^{\rm FCM}$, for the (c) 'full ring' and (d) 'normal ring' at various z-positions during for the final step (10th step) of FCM from 22 T.

inset of each figure shows the contour map of the $\sigma_\theta^{\rm cool}$ profile. In figure 5(a), a large compressive stress ($\sigma_\theta < 0$) is thermally applied to the disk bulk region ($r \leqslant 10$ mm) and the tensile stress is applied to the SUS316 ring, because the thermal expansion coefficient, α, of the SUS316 is about 2.5 times larger than that of the REBaCuO bulk, as shown in table 1. The $\sigma_\theta^{\rm cool}$ values for the bulk center ($z = 6.5$ mm, $r = 0$ mm) and bulk surface ($z = 1.6$ or 11.4 mm, $r = 0$ mm) are -195 and -137 MPa, respectively. On the other hand, in figure 5(b), the $\sigma_\theta^{\rm cool}$ values of the 'normal ring' case at the bulk center ($r = 0$ mm) are smaller than those of the 'full ring' case. It is surprising that the compressive $\sigma_\theta^{\rm cool}$ value near the bulk surface ($z = 1.6$ and 11.4 mm) drastically decreases at the bulk periphery ($r = 9$ mm). Because of the larger α value of the SUS316 compared to the bulk, the SUS316 ring shrinks along both z- and r-directions. The bulk was fastened along the r-direction and, at the same time, the periphery region of the bulk was pulled toward the bulk center ($z = 6.5$ mm). As a result, the compressive hoop stress around the bulk periphery became weak [28].

The electromagnetic hoop stress, $\sigma_\theta^{\rm FCM}$, for the 'full ring' and the 'normal ring' cases was simulated for each step of FCM from 22 T without cooling (only FCM). The $\sigma_\theta^{\rm FCM}$ value distributes in the bulk and changes with increasing TS. Figure 6(a) shows the TS dependence of the $\sigma_\theta^{\rm FCM}$ values at the position of $(r, z) = (0.5, 11.4$ mm) for the 'full ring' and the 'normal ring' cases under $J_c = 4J_c{}^*$, $3J_c{}^*$ and $2J_c{}^*$ during FCM from 22 T. Since the $\sigma_\theta^{\rm FCM}$ value on the z-axis ($r = 0$ mm) cannot be strictly obtained due to the critical point in the numerical model, $\sigma_\theta^{\rm FCM}$ values at $(r, z) = (0.5, 11.4$ mm) were substituted. The $\sigma_\theta^{\rm FCM}$ value took a maximum at the center of the bulk surface for all cases. These tendencies were also obtained for the similar simulation [8, 28]. The $\sigma_\theta^{\rm FCM}$ value for the 'full ring' case gradually increases with increasing TS, and with increasing J_c value of the bulk. For the $J_c = 2J_c{}^*$ case, the $\sigma_\theta^{\rm FCM}$ value took a maximum at the seventh step and decreased with the further increase in *TS*, which result from the decrease of the trapped field. On the other hand, the $\sigma_\theta^{\rm FCM}$ value for the 'normal ring' case is about twice as large as that for the 'full ring' case because the 'normal ring' reinforcement effect is weaker at the bulk surface [28]. Figure 6(b) shows the similar TS dependence of the $\sigma_\theta^{\rm FCM}$ value at the position of $(r, z) = (0.5, 6.5$ mm) of the bulk center. The $\sigma_\theta^{\rm FCM}$ value hardly changes depending on the J_c value due to the sufficient reinforcement at the bulk center, and the difference between the 'full ring' and the 'normal ring' cases was relatively small.

Figures 6(c) and (d), respectively, show the radius (r) dependence of the electromagnetic hoop stress, $\sigma_\theta^{\rm FCM}$, for the 'full ring' and the 'normal ring' cases at various z-positions

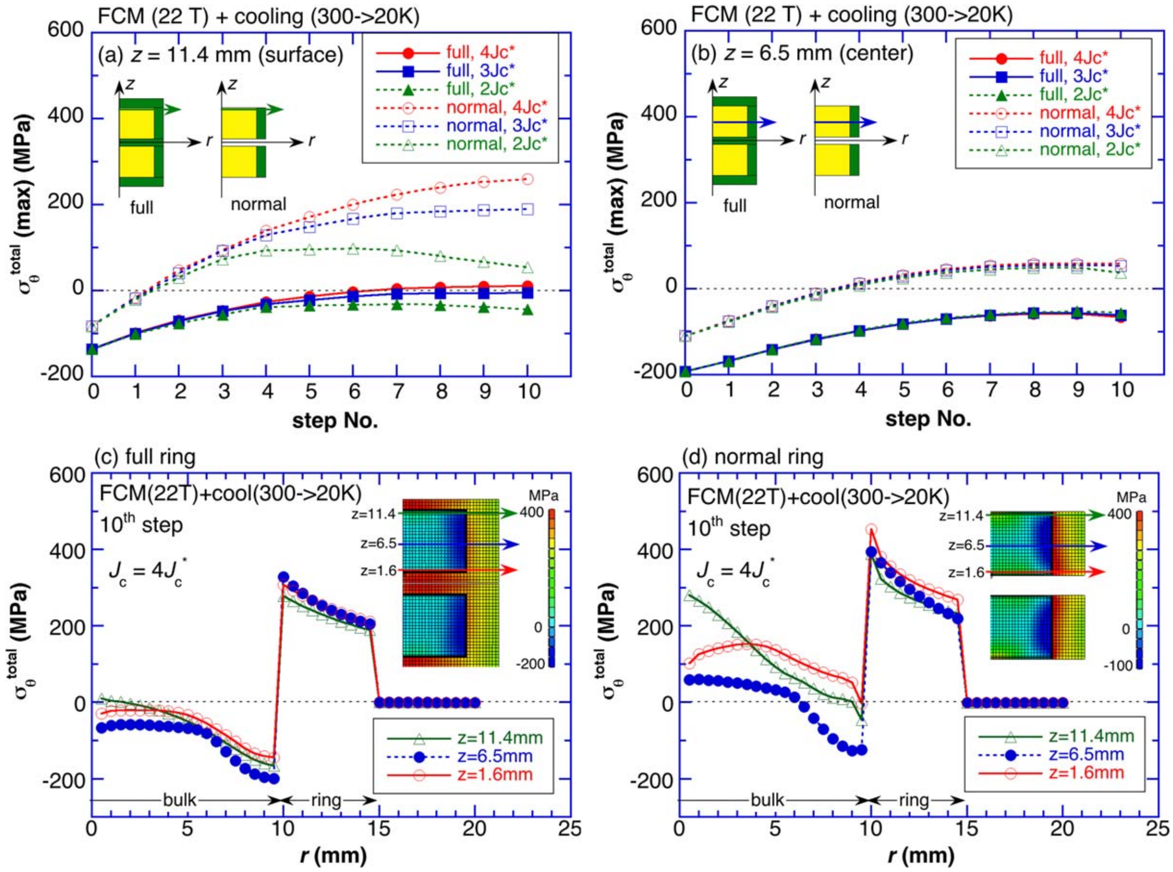

Figure 7. The TS dependence of the $\sigma_\theta{}^{\text{total}}$ values at the positions of (a) $(r, z) = (0.5\ \text{mm}, 11.4\ \text{mm})$ and (b) $(r, z) = (0.5\ \text{mm}, 6.5\ \text{mm})$ for the 'full ring' and the 'normal ring' cases under $J_c = 2J_c^*$, $3J_c^*$ and $4J_c^*$ during FCM from 22 T. The radius (r) dependence of the $\sigma_\theta{}^{\text{total}}$, for the (c) 'full ring' and (d) 'normal ring' at various z-positions during for the final step (10th step) of FCM from 22 T.

during for the final step (10th step) of FCM from 22 T without cooling (only FCM). The inset of each figure shows the contour map of the $\sigma_\theta^{\text{FCM}}$ profile. In figure 6(c), the $\sigma_\theta^{\text{FCM}}$ value was larger at the central region and the z dependence of the $\sigma_\theta^{\text{FCM}}$ value is relatively small. On the other hand, for the 'normal ring' case, the $\sigma_\theta^{\text{FCM}}$ values at the bottom ($z = 1.6$ mm) and top ($z = 11.4$ mm) surfaces were enhanced because of the reduction of the reinforcement effect at the bulk surface. The r dependences of the $\sigma_\theta^{\text{FCM}}$ are quite different and asymmetric between $z = 1.6$ and 11.4 mm, which result from the influence of other magnetized bulk.

Figure 7(a) shows the TS dependence of the maximum total hoop stress, $\sigma_\theta{}^{\text{total}}(\text{max})$ $(= \sigma_\theta^{\text{FCM}} + \sigma_\theta^{\text{cool}})$, for the 'full ring' and the 'normal ring' cases under $J_c = 4J_c^*$, $3J_c^*$ and $2J_c^*$ during FCM from 22 T at the position of $(r, z) = (0.5, 11.4\ \text{mm})$, at which the maximum hoop stress is applied during FCM process. The $\sigma_\theta^{\text{total}}(\max)$ value is smaller than the $\sigma_\theta^{\text{FCM}}$ value as shown in figure 6(a) because of the compressive effect of the metal ring by cooling. For the 'normal ring' case, the $\sigma_\theta^{\text{total}}(\max)$ value was as high as +100 MPa at the fifth step even for the $J_c = 2J_c^*$ case and increased with increasing J_c value, in which the bulk of the 'normal ring' must be broken if the fracture strength of the typical Ag-doped REBaCuO bulk is 50–70 MPa [16–18]. On the other hand, for the 'full ring' case, the $\sigma_\theta^{\text{total}}(\max)$ value was only +10 MPa even for the $J_c = 4J_c^*$ case, which suggests that the bulk might not break because of the effective mechanical reinforcement.

Figure 7(b) shows the similar TS dependence of the $\sigma_\theta^{\text{total}}(\max)$ value at the position of $(r, z) = (0.5\ \text{mm}, 6.5\ \text{mm})$ of the bulk center. The $\sigma_\theta^{\text{total}}(\max)$ value hardly changes depending on the J_c value due to the sufficient reinforcement effect at the bulk center. The $\sigma_\theta^{\text{total}}(\max)$ value for the 'full ring' case is negative (compressive stress) during FCM step. For the 'normal ring' case, the maximum $\sigma_\theta^{\text{total}}$ value was drastically reduced to be +45 MPa by the cooling reinforcement, compared with the maximum $\sigma_\theta^{\text{FCM}}$ value of +180 MPa shown in figure 6(b).

Figures 7(c) and (d), respectively, show the radius dependence of the total hoop stress, $\sigma_\theta^{\text{total}}$ $(= \sigma_\theta^{\text{FCM}} + \sigma_\theta^{\text{cool}})$, for the 'full ring' and the 'normal ring' cases at various z-positions during for the final step (10th step) of FCM from 22 T. The inset of each figure shows the contour map of the $\sigma_\theta^{\text{total}}$ profile. In figure 7(c), the $\sigma_\theta^{\text{total}}$ value was larger at the central region ($r = 0$ mm) and the z dependence of the $\sigma_\theta^{\text{total}}$ value is relatively small. The similar $\sigma_\theta^{\text{total}}$ profile can be seen for each *TS*. On the other hand, for the 'normal ring' case shown in figure 7(d), the $\sigma_\theta^{\text{total}}$ value at the bottom ($z = 1.6$ mm) and top ($z = 11.4$ mm) surfaces was enhanced because of the reduction of the reinforcement effect of the

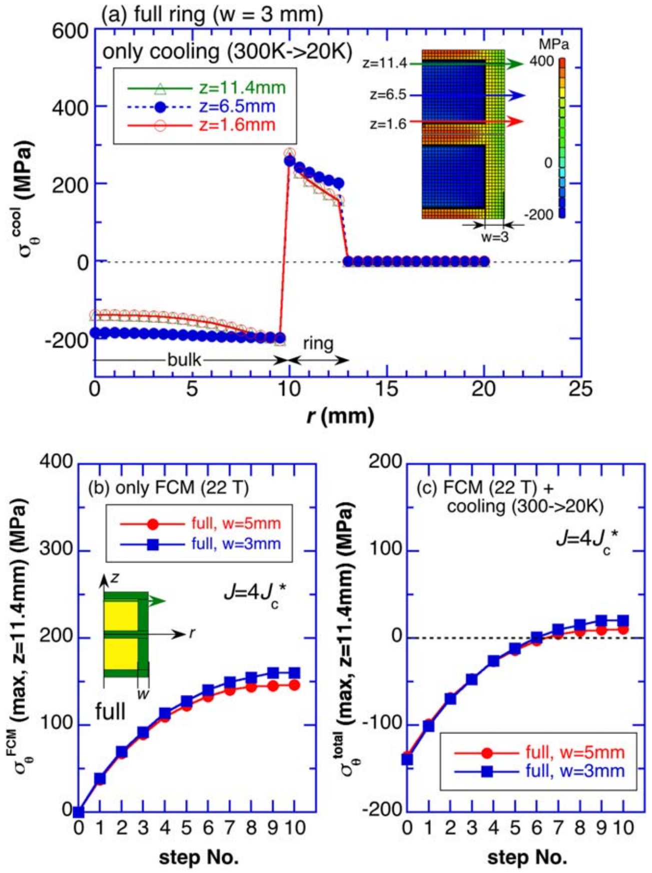

Figure 8. (a) The radius (r) dependence of the thermal hoop stress, $\sigma_\theta{}^{cool}$, for the 'full ring' with $w = 3$ mm at various z-positions under the cooling from 300 K to 20 K without FCM (only cooling). The time step dependence of the (b) $\sigma_\theta{}^{cool}$ and (c) $\sigma_\theta{}^{total}$ values at $z = 11.4$ mm for the $w = 3$ mm bulk, compared with those for the $w = 5$ mm bulk.

normal ring. The 0.2% proof stress of SUS316 is about 600 MPa at 77 K, which changes depending on the carbon and nitrogen contents in the material [36]. The maximum stress applied at the inner periphery of the SUS316 ring shown in figures 7(c) and (d) was smaller than that value. The SUS316 part used in the study can reinforce the bulk within the 0.2% proof stress safely.

3.3. Effect of the width of outer SUS316 ring

In the previous subsection, we presented the effect of the new reinforcement structure of the metal ring, in which the width of the outer SUS316 ring was $w = 5$ mm, as shown in figure 1. Finally, we investigate the influence of the outer ring width, w, on the compressive stress during cooling, σ_θ^{cool}, and total hoop stress, σ_θ^{total} during FCM. Figure 8(a) shows the radius (r) dependence of the thermal hoop stress, σ_θ^{cool}, for the 'full ring' with $w = 3$ mm at various z-positions under the cooling from 300 K to 20 K without FCM (only cooling). The tensile stress in the SUS316 ring with $w = 3$ mm was $\sigma_\theta^{cool} = 250$ Mpa at $r = 10.5$ mm, which is larger than that the tensile stress $\sigma_\theta^{cool} = 200$ Mpa obtained for $w = 5$ mm, as shown in figure 5(a). However, the compressive stress in the bulk part with $w = 3$ mm is nearly the same as the $w = 5$ mm case. Figures 8(b) and (c), respectively, show the TS dependence of the σ_θ^{FCM} and σ_θ^{total} values for the $w = 3$ mm bulk, compared to those for the $w = 5$ mm bulk. These values for the $w = 3$ mm are slightly larger than those for the $w = 5$ mm bulk. However, the σ_θ^{total} value is fairly smaller than the fracture strength of the REBaCuO bulk material of 50 $\sim$ 70 MPa [16–18]. These results suggest that the width of $w = 3$ mm is sufficient to reinforce the bulk and to prevent the bulk fracture during FCM up to 22 T, and that the diameter of the REBaCuO bulk could be slightly increased, in which the restriction with higher $J_c(B)$ of the bulk can be relaxed to achieve higher trapped field over 20 T.

4. Conclusion

We proposed an effective mechanical reinforcement structure for REBaCuO superconducting disk bulk pair to avoid mechanical fracture during FCM from 22 T, and confirmed the reinforcement effect using numerical simulation. The important results and conclusions are summarized as follows.

(1) A higher trapped field, B_z, over 20 T can be achieved in the gap center of the bulk pair, which was fully encapsulated by outer ring and upper and lower plates made by SUS316.
(2) A large compressive hoop stress, σ_θ^{cool}, due to the difference of thermal expansion coefficient between the bulk and SUS316, was effectively applied to the whole bulk during the cooling process from 300 K to 20 K, compared to that for the conventional reinforcement using only a SUS316 ring.
(3) The electromagnetic hoop stress, $\sigma_\theta{}^{FCM}$, during FCM was also reduced and the maximum of the total hoop stress, σ_θ^{total}(max) (= $\sigma_\theta{}^{FCM} + \sigma_\theta^{cool}$) can be reduced to +10 MPa by the proposed reinforcement structure, which was lower than the mechanical strength of the typical Ag-doped REBaCuO bulk (50–70 MPa). The possibility to achieve higher trapped field over 20 T was suggested in the gap in the REBaCuO bulk pair without fracture.

Acknowledgments

This work was performed at the High Field Laboratory for Superconducting Materials (HFLSM), Institute for Materials Research, Tohoku University (Project No. 18H0055), and was partially supported by JSPS KAKENHI grant No. JP15K04646.

ORCID iDs

Hiroyuki Fujishiro https://orcid.org/0000-0003-1483-835X
Tomoyuki Naito https://orcid.org/0000-0001-7594-3466

References

[1] Shi Y-H, Hari Babu N, Iida K, Yeoh W K, Dennis A R, Pathak S K and Cardwell D A 2010 *Physica* C **470** 685–8
[2] Muralidhar M, Sakai N, Jirsa M, Koshizuka N and Murakami M 2004 *Appl. Phys. Lett.* **85** 3504

[3] Isfort D, Chaud X, Tournier R and Kapelski G 2003 *Physica* C **390** 341–55
[4] Chaud X, Noudem J, Prikhna T, Savchuk Y, Haanappel E, Diko P and Zhang C P 2009 *Physica* C **469** 1200–6
[5] Prikhna T A, Rabier J, Proult A, Chaud X, Gawalek W, Vlasenko A V, Soubeyroux J-L, Tournier R, Sandiumenge F and Savchuk Ya M 2004 *Supercond. Sci. Technol.* **17** S515
[6] Diko P, Chaud X, Antal V, Kanuchova M, Sefclkova M and Kovac J 2008 *Supercond. Sci. Technol.* **21** 115008
[7] Kenfaui D, Sibeud P F, Louradour E, Chaud X and Noudem J G 2014 *Adv. Funct. Mater.* **24** 3996–4004
[8] Ren Y R, Weinstein R, Liu J, Sah R P and Foster C 1995 *Physica* C **251** 15
[9] Mochizuki H, Fujishiro H, Naito T, Itoh Y, Yanagi Y and Nakamura T 2016 *IEEE Trans. Appl. Supercond.* **26** 6800205
[10] Schatzle P, Krabbes G, Gruss S and Fuchs G 1999 *IEEE Trans. Appl. Supercond.* **9** 2022
[11] Lee D and Salama K 1990 *Japan. J. Appl. Phys.* **29** L2017
[12] Nariki S, Sakai N, Tomita M and Murakami M 2002 *Physica* C **378-381** 779–82
[13] Tomita M and Murakami M 2003 *Nature* **421** 517–20
[14] Tomita M, Murakami M and Katagiri K 2002 *Physica* C **378-381** 783–7
[15] Tomita M and Murakami M 2003 *Physica* C **392-396** 562–6
[16] Murakami A, Miyata H, Hashimoto R, Katagiri K and Iwamoto A 2009 *IEEE Trans. Appl. Supercond.* **19** 2995–8
[17] Murakami A, Miyata H, Hashimoto R, Katagiri K and Iwamoto A 2008 *Physica* C **468** 1395–8
[18] Fujimoto H, Murakami A, Teshima H and Morita M 2013 *Cryogenics* **57** 6–11
[19] Murakami A, Fujimoto H and Iwamoto A 2012 *Phys. Proc.* **27** 160–3
[20] Kenfaui D, Sibeud P-F, Gomina M, Louradour E, Chaud X and Noudem J G 2015 *J. Phys. Chem. Lett.* **6** 2999–3005
[21] Fuchs G, Schatzle P, Krabbes G, Gruss S, Verges P, Muller K-H, Fink J and Schultz L 2000 *Appl. Phys. Lett.* **76** 2107
[22] Gruss S, Fuchs G, Krabbes G, Verges P, Stover G, Muller K-H and Fink J 2001 *Appl. Phys. Lett.* **79** 3131–3
[23] Durrell J H *et al* 2014 *Supercond. Sci. Technol.* **27** 082001
[24] Johansen T, Wang C, Chen Q Y and Chu W–K 2000 *J. Appl. Phys.* **88** 2730–3
[25] Johansen T 2000 *Supercond. Sci. Technol.* **13** R121–37
[26] Johansen T 1999 *Phys. Rev.* B **60** 9690–703
[27] Huang C, Yong H and Zhou H 2013 *Supercond. Sci. Technol.* **26** 105007
[28] Fujishiro H, Ainslie M D, Takahashi K, Naito T, Yanagi Y, Itoh Y and Nakamura T 2017 *Supercond. Sci. Technol.* **30** 085008
[29] Takahashi K, Fujishiro H, Naito T, Yanagi Y, Itoh Y and Nakamura T 2017 *Supercond. Sci. Technol.* **30** 115006
[30] Fujishiro H, Takahashi K, Naito T, Yanagi Y, Itoh Y and Nakamura T 2018 *Physica* C **550** 52–6
[31] Hughes D D 2001 *Low Temp. Phys.* **27** 713–22
[32] Kii T *et al* 2012 *IEEE Trans. Appl. Supercond.* **22** 4100904
[33] Meng R L, Gao L, Gautier-Picard P, Ramirez D, Sun Y Y and Chu C W *Physica* C **232** 337–46
[34] Ainslie M D and Fujishiro H 2015 *Supercond. Sci. Technol.* **28** 053002
[35] Ainslie M D, Zhou D, Fujishiro H, Takahashi K, Shi Y-H and Durrell J 2016 *Supercond. Sci. Technol.* **29** 124004
[36] Simon N J and Reed R P 1988 *Advances in Cryogenic Engineering—Materials* p 165(New York: Plenum Press)